

apter]schemelosScheme

**University of São Paulo  
São Carlos School of Engineering**

**Guilherme Soares Silvestre**

**Robotic-Assisted SEEG for Epilepsy: A Phantom-Based  
Accuracy Study of the Yara Platform**

**São Carlos**

**2025**



**Guilherme Soares Silvestre**

## **Robotic-Assisted SEEG for Epilepsy: A Phantom-Based Accuracy Study of the Yara Platform**

Monografia apresentada ao Curso de Engenharia Mecatrônica, da Escola de Engenharia de São Carlos da Universidade de São Paulo, como parte dos requisitos para obtenção do título de Engenheiro Mecatrônico.

Advisor: Prof. Dr. Glauco Augusto de Paula Caurin

**São Carlos  
2025**



## **ACKNOWLEDGEMENTS**







## **ABSTRACT**

**Silvestre, G.S. Robotic-Assisted SEEG for Epilepsy: A Phantom-Based Accuracy Study of the Yara Platform.** 2025. 46p. Monograph (Conclusion Course Paper) - University of São Paulo, São Carlos, 2025.

This research introduces a novel concept for a robotic system, Yara, specifically designed for Stereoelectroencephalography (SEEG) neurosurgery. The platform integrates collaborative robotic assistance, leveraging the precision of robotic systems, and is adaptable to various surgical environments. The study evaluates the system's final accuracy by replicating a SEEG neurosurgery procedure on a 3D reconstructed patient. The patient's head, cranium, and brain models were reproduced using different materials derived from tomography. The surgical procedure was simulated, starting from planning, proceeding through fiducial registration, and culminating with electrode placement. A post-operative tomography was performed to compute the error between the planned electrode trajectories and the final position of each entry and target point, providing a comprehensive assessment of the system's accuracy and effectiveness in SEEG neurosurgery.

**Keywords:**



## RESUMO

Silvestre, G.S. **Robotic-Assisted SEEG for Epilepsy: A Phantom-Based Accuracy Study of the Yara Platform.** 2025. 46p. Monografia (Trabalho de Conclusão de Curso) - University of São Paulo, São Carlos, 2025.



## LIST OF FIGURES

Figure 1 – Positioning of electrodes in scalp electroencephalography, electrocorticography, and stereoelectroencephalography procedures respectively (SHEN, 2020) (Blausen.com staff, 2014) (JONES <i>et al.</i> , 2018). . . . .	24
Figure 2 – (a) presents Tilarach's <i>frame</i> with x-ray supports and (b) presents an example x-ray image alongside the coordinate system developed by Tilarach (MAZOYER, 2008). . . . .	25
Figure 3 – Frame Leksell G without N-Localizer and with N-Localizer respectively (ROJAS-VILLABONA <i>et al.</i> , 2016). . . . .	26
Figure 4 – Robots capable of performing SEEG surgeries: Zimmer Biomet ROSA ONE Brain, Brainlab Cirq and Renishaw Neuromate respectively. . . . .	28
Figure 5 – Conical targets phantom used for quantitative accuracy assessment via stereoscopic imaging. . . . .	36
Figure 6 – Conical targets phantom in simulated environment for metal rods positioning using the robotic system. . . . .	36
Figure 7 – Examples of stereo camera images used to measure the distance between the metal rod tip and the planned target point. The top and bottom rows show the left and right images of a stereo pair for the same moment in time. . . . .	37
Figure 8 – Phantom model with synthetic brain produced using silicone rubber and 3D printed plastic surface skin after electrode placement. . . . .	37
Figure 9 – Synthetic brain phantom in the simulated environment during electrode placement with the robotic system. The rightmost image displays the postoperative CT scan of inserted electrodes. . . . .	38
Figure 10 – Comparison between preoperative (red and green lines) and postoperative (gray contacts) electrode trajectories using CT scan of the synthetic brain model in the simulated environment. . . . .	39
Figure 11 – Phantom model with synthetic brain placed in the surgical room using stereotactic frame for electrode placement. . . . .	39
Figure 12 – Comparison between frame-based planned electrode trajectories (color lines) and those achieved after surgery (showed by the sliced view of the contacts in bright gray) using CT scan of a synthetic brain model in OR with stereotactic frame. . . . .	40
Figure 13 – Operating room (OR) with synthetic brain phantom ready for electrode placement using the robotic system. . . . .	41
Figure 14 – Electrodes fixed to the synthetic brain phantom in OR with robotic system. . . . .	41

Figure 15 – Comparison between planned electrode trajectories (red and green lines) and those achieved after surgery (3D contacts in gray) using CT scan of a synthetic brain model in OR with robotic system. . . . . 42

## **LIST OF ABBREVIATIONS AND ACRONYMS**

SEEG - Stereoeletroencefalography

ROS - Robot Operating System



## CONTENTS

1	<b>INTRODUCTION . . . . .</b>	17
2	<b>OBJECTIVES . . . . .</b>	19
3	<b>LITERATURE REVIEW . . . . .</b>	21
3.1	<b>Epilepsy . . . . .</b>	21
3.2	<b>Treatment Methods . . . . .</b>	22
3.2.1	Non-invasive Video-EEG . . . . .	22
3.2.2	Invasive EEG: Subdural EEG (SDE) and Stereoencephalography (SEEG) . . . . .	23
3.3	<b>Stereoelectroencephalography: Operation Methods . . . . .</b>	24
3.3.1	Stereotaxy And SEEG . . . . .	24
3.3.2	Frame-based Surgeries . . . . .	25
3.3.3	Robot-based Surgeries . . . . .	28
3.4	<b>Introducing Yara . . . . .</b>	29
4	<b>DEVELOPMENT . . . . .</b>	31
4.1	<b>Patient Monitoring Phase . . . . .</b>	31
4.2	<b>SEEG Planning Phase . . . . .</b>	31
4.2.1	Image Fusion . . . . .	32
4.2.2	Electrode Placement . . . . .	32
4.3	<b>Robot-Scan Registration Phase . . . . .</b>	32
4.4	<b>Intra-Operation Phase . . . . .</b>	34
5	<b>METHOD AND RESULTS . . . . .</b>	35
5.1	<b>Conical Target Phantom in Simulated Environment . . . . .</b>	35
5.2	<b>Synthetic Brain Phantom in Simulated Environment . . . . .</b>	37
5.3	<b>Synthetic Brain Phantom in Surgical Room . . . . .</b>	39
6	<b>DISCUSSION AND CONCLUSION . . . . .</b>	43
	<b>REFERENCES . . . . .</b>	45



## 1 INTRODUCTION

In cranial neurosurgery, intracranial electrode placement is a core procedure for both diagnostic and therapeutic purposes, particularly in the management of epilepsy and movement disorders. These procedures require the accurate insertion of electrodes into specific brain regions to record neural activity or deliver stimulation, reason why robotic assistance is increasingly utilized. Among the most common applications are stereoelectroencephalography (SEEG) for epilepsy diagnosis and deep brain stimulation (DBS) for treating movement disorders such as Parkinson's disease.

SEEG involves the implantation of multiple depth electrodes into targeted brain areas to localize epileptogenic zones that are responsible for seizure generation. This technique provides critical information for surgical planning in drug-resistant epilepsy cases. In contrast, DBS is a therapeutic intervention where electrodes are implanted into subcortical structures, such as the subthalamic nucleus or globus pallidus, to deliver electrical stimulation that modulates abnormal neural circuits. DBS has become a standard treatment for movement disorders, notably Parkinson's disease, essential tremor, and dystonia, offering significant improvements in motor symptoms and quality of life for affected patients.

Robotic systems are increasingly being adopted for intracranial electrode implantation by maintaining accuracy and enhancing surgical workflow. Neuromate, introduced in the late 1990s, was among the first dedicated robotic platforms for neurosurgery, enabling automated and precise placement of electrodes for procedures such as SEEG and DBS. The subsequent development of ROSA brought further advancements, expanding its applications to include spine surgery and other orthopedic interventions. In epilepsy surgery, robotic assistance has proven particularly valuable, offering similar accuracy in localizing and targeting epileptogenic zones comparable to traditional methods, while significantly reducing operative time (KAEWBORISUTSAKUL *et al.*, 2024).

This work proposes the development of a collaborative robotic system for precise intracranial electrode placement during SEEG procedures in the treatment of epilepsy. To contextualize this objective, it is essential to review the clinical features of epilepsy (Section 3.1), the classification and impact of seizure types, and the current therapeutic strategies available (Section 3.2).



## 2 OBJECTIVES

The objective of this work is to evaluate the accuracy of the proposed collaborative robotic system for intracranial electrode placement during SEEG procedures. This evaluation will be conducted using anatomical phantoms that simulate human cranial structures, allowing for precise measurement of electrode placement accuracy and assessment of the system's potential to improve surgical outcomes in epilepsy treatment.



### 3 LITERATURE REVIEW

#### 3.1 Epilepsy

*Epilepsy* is a chronic brain disease characterized by a long-lasting predisposition to generate seizures, not caused by any immediate insult to the central nervous system, and by the neurobiological, cognitive, psychological, and social consequences of recurrent seizures (BEGHI, 2020). This is the most common neurological disease worldwide, affecting different social classes, races, ages, and geographic locations (NGUGI *et al.*, 2010).

The definition of epileptic seizures is: repeated and transient episodes that manifest themselves through patterned behaviors, mirroring the underlying neural processes associated with the condition (FISHER *et al.*, 2005). Although all people with epilepsy experience seizures, not all individuals with seizures have epilepsy. Epileptic seizures can also occur after an acute injury to the central nervous system (CNS) of structural, systemic, toxic, or metabolic origin. These events are considered acute manifestations of the insult and may not occur when the underlying cause has been removed or the acute phase has passed (BEGHI *et al.*, 2010).

Epileptic seizures are categorized according to three main characteristics: origin in the brain, state of consciousness during the seizure, and level of body movement. Seizures can be classified as focal or generalized based on the first characteristic. The second characteristic considers whether consciousness is intact or impaired during the seizure, while the third characteristic refers to body movement, which may present motor or non-motor reactions (BEGHI, 2020).

Motor seizures encompass a variety of distinct manifestations. Atonic crises are characterized by a sudden and temporary loss of muscle tone, resulting in a sudden fall of the individual. On the other hand, tonic crises involve a sudden and prolonged increase in muscle tone, leading to intense stiffness. Clonic seizures are marked by rhythmic and repetitive muscle contractions, which can affect different parts of the body, while myoclonic seizures are characterized by rapid and sudden muscle contractions that can involve a specific muscle group or the entire body. Epileptic spasms, automatisms, and hyperkinetic seizures are also categorized (SARMAST; ABDULLAHI; JAHAN, 2020).

On the other hand, non-motor crises can present different forms of manifestation. They can be autonomic, involving dysfunctions in the autonomic nervous system, such as changes in blood pressure or heart rate. In addition, there may be crises of behavioral arrest, during which the individual may appear paralyzed or unable to perform voluntary movements. Cognitive crises affect cognitive function and may include memory lapses or mental confusion. Emotional crises are related to changes in the emotional state, such as

feelings of fear, anxiety, or euphoria. Finally, sensory crises affect the senses and can cause abnormal sensations, such as visual or auditory hallucinations (SARMAST; ABDULLAHI; JAHAN, 2020).

### 3.2 Treatment Methods

Among patients with epilepsy, approximately 30% experience drug-resistant seizures, representing a significant portion of the global population, estimated at 70 million people. In such cases, resective surgery may be considered as a therapeutic option. This procedure is indicated for patients with disabling focal epilepsy who are unresponsive to drug treatment and whose seizures originate in a specific region of the brain that can be removed with minimal risk of neurological or cognitive dysfunction (MILLER; HAKIMIAN, 2013). Resective surgery offers the possibility of significantly improving the quality of life of these patients, providing adequate control of seizures and reducing dependence on high-cost and potentially harmful antiepileptic medications.

Correctly locating the focus of seizures is a crucial aspect in preparing for resective surgery in patients with epilepsy (MILLER; HAKIMIAN, 2013). Localization methods are applied to accurately determine the focal region, aiming to minimize the invasiveness of the surgery while seeking complete removal of the area of focus to cease seizures. Accuracy in locating the focus has a significant impact on the effectiveness of the surgical procedure, as it can help avoid undesirable consequences associated with the resection of unaffected areas.

This is especially important, as the removal of critical areas of the brain can result in functional deficits, such as impairment of speech, memory, motor coordination, among other functions, depending on the location of the focus. Therefore, ensuring accurate location of the focus is essential to guarantee good surgical results and minimize potential adverse effects.

#### 3.2.1 Non-invasive Video-EEG

Before progressing to invasive procedures, a non-invasive analysis is typically performed to identify potential areas of seizure foci and to guide further investigation. Scalp EEG is the primary non-invasive technique used for this purpose. Electrodes are placed on the patient's scalp using a cap or similar device, enabling monitoring during interictal (between seizures), ictal (during seizures), and post-ictal (after seizures) periods. This superficial electrode arrangement measures electrical potentials generated by neuronal activity near the skull. Standard systems use 32, 64, or 96 electrodes distributed across the scalp, with higher-density arrays (up to 256 channels) available for more detailed studies (SUN; MOU, 2023). Scalp EEG is essential for initial diagnosis and localization of seizure

activity, providing critical information before invasive methods are considered (MILLER; HAKIMIAN, 2013).

### 3.2.2 Invasive EEG: Subdural EEG (SDE) and Stereoencephalography (SEEG)

Subdural EEG (SDE), also known as electrocorticography (ECoG), was developed to provide more precise measurement of brain activity than scalp EEG. In SDE, an electrode array is placed directly on the surface of the cortex after a portion of the skull is removed, as illustrated in Fig. 1. This direct contact enables the acquisition of signals with higher fidelity and less noise compared to scalp EEG (LESSER; CRONE; WEBBER, 2010). The electrodes typically remain in place for several days to record both ictal and interictal activity. However, SDE is highly invasive, requiring two craniotomies — one for electrode placement and another for removal — and carries a significant risk of postoperative infection, often related to surgical contamination. These drawbacks have motivated the development of alternative methods, such as SEEG, which aim to reduce invasiveness and associated complications (JEHI *et al.*, 2021).

In France, in the 1950s, Jean Tilarach and Jean Bancaud developed a method that aims to monitor deep parts of the cortex through the insertion of deep electrodes, seeking to replace the SDE (MAZOYER, 2008). This method was called Stereoelectroencephalography (SEEG) and today it is one of the most adopted invasive methods for locating the focal zone of seizures. SEEG does not present many of the problems presented by SDE. In this method, cylindrical electrodes (more like small wires) are introduced through small holes in the skull, without the need for craniotomy. SEEG has lower rates of infection, hemorrhage, neurological deficits, and morbidity compared to SDE, in addition to being a faster procedure, allowing the analysis of deeper brain tissues and having shown greater effectiveness in localizing and controlling seizures after surgical treatment (FIANI *et al.*, 2021). Fig. 1 illustrates the positioning of electrodes in scalp EEG, Subdural EEG (electrocorticography), and SEEG.

Electrodes implanted by SEEG must be precisely placed for proper identification of the epileptogenic zone (EZ) (JONES *et al.*, 2018). Planning prior to surgery is carried out to define the number of electrodes, the position of the entry points, and the target point of each electrode. Metrics are defined for evaluating the effectiveness of SEEG operations, constituting a basis for evaluating different SEEG methods. Entry points are defined as the point at which the electrode initiates contact with the surface of the brain. Target points are defined as the final position of the electrode, usually in a region within the brain.

Widely adopted metrics for evaluating the accuracy of the electrode placement are the Euclidean distance between the planned entry points and the post-surgical entry points, the distance between the planned target points and the post-surgical target points,

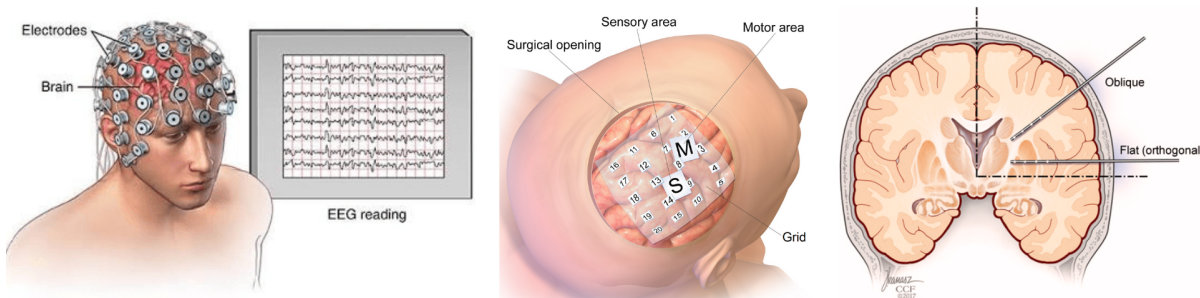


Figure 1 – Positioning of electrodes in scalp electroencephalography, electrocorticography, and stereoelectroencephalography procedures respectively (SHEN, 2020) (Blausen.com staff, 2014) (JONES *et al.*, 2018).

and the angle between the two vectors formed by the planned and post-surgical entry and target points representing the orientation error.

### 3.3 Stereoelectroencephalography: Operation Methods

#### 3.3.1 Stereotaxy And SEEG

SEEG operation techniques began with Tilarach using x-ray images for planning and checking electrode positioning. Since the inception of SEEG, the development of mechanical stereotaxic apparatus that fix the skull and guide electrode placement has been the focus to achieve the best accuracy during surgery. The first apparatus was called the Tilarach apparatus and featured pins for fixing the skull, support for the x-ray tube, and radiographic film (MAZOYER, 2008). Popular devices today date their creation to the same time, such as the Leksell in Sweden.

With the advent of computed tomography, surgeries began to be planned based on slices, allowing a three-dimensional understanding of the areas of investigation. Devices that use the three-dimensionality of tomography images were adapted, adding a support with a diagonal cut in the shape of an N, allowing the calculation of the height of each tomography slice in relation to the device coordinates. This system became known as the N-Localizer and is widely used in current neurosurgeries (LOZANO *et al.*, 2009).

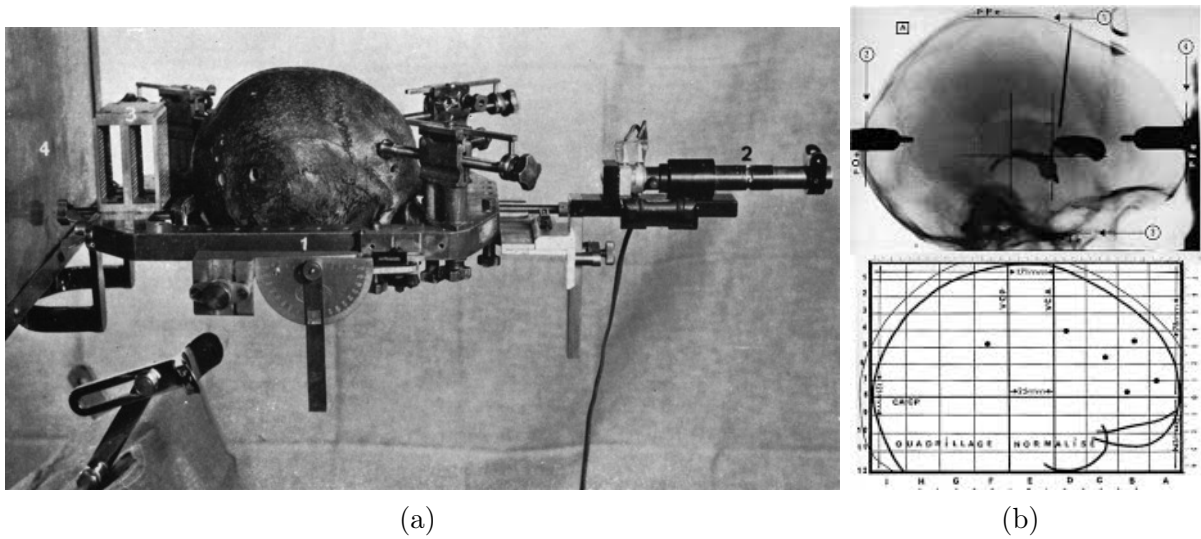


Figure 2 – (a) presents Talairach’s *frame* with x-ray supports and (b) presents an example x-ray image alongside the coordinate system developed by Talairach (MAZOYER, 2008).

### 3.3.2 Frame-based Surgeries

The earliest SEEG technique involved introducing electrodes in parallel trajectories, normal to the sagittal view, using the Cartesian map called Talairach coordinates (MAZOYER, 2008). Subsequently, variations of the technique were explored with the introduction of stereotaxic arcs that can be fixed to devices such as the Leksell or CRW and that allow the introduction of oblique electrodes. Therefore, the assessment of the impact on precision between different techniques for implanting oblique or orthogonal electrodes was studied in (IORDANOU *et al.*, 2019). Figure 3 presents the Leksell G apparatus and the N-Localizer.

Originally, the calculation of the coordinates of each electrode in relation to the apparatus was carried out manually, using the N-Localizer geometry. Software for surgical planning was developed so that the calculation of the coordinates of the entry and target points was automated using image processing methods containing the N-Localizer (DASGUPTA *et al.*, 2022). These software also features planning tools, such as fusing standard CT images and MRI images.

Image fusion allows precise surgical planning by combining preoperative CT and MRI scans to assess vascular structures and functional anatomy near electrode trajectories. During surgery, a stereotactic frame and N-Localizer are attached to the patient’s head, followed by an intraoperative CT scan. This scan is fused with the preoperative images, enabling the planning software to identify N-Localizer fiducials and accurately compute coordinates for electrode placement. These coordinates are then inputted into the stereotactic frame or arc, guiding the surgeon in positioning each electrode along the planned trajectory.

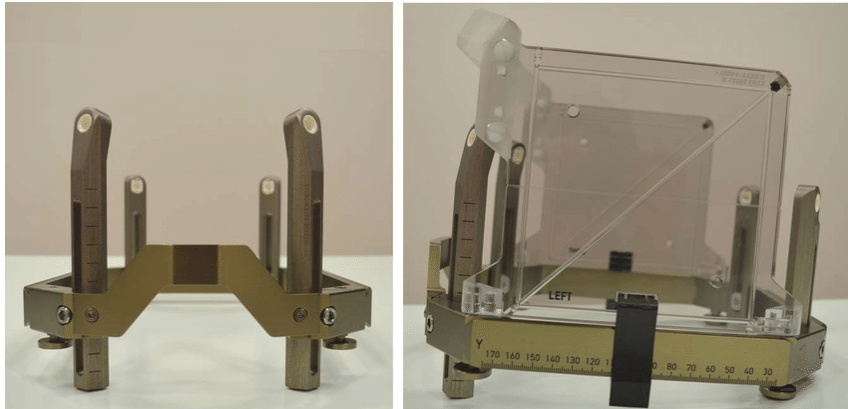


Figure 3 – Frame Leksell G without N-Localizer and with N-Localizer respectively (ROJAS-VILLABONA *et al.*, 2016).

Surgeries based on stereotactic devices have a broad history of use, but they also have disadvantages in relation to more recent systems, such as robotic systems. Among the disadvantages, the stereotactic frames operation requires the placement of the apparatus at the beginning of the surgery, followed by a CT with the N-Localizer generally located in another room, and the fusion of this CT to the MRI taken (generally days before surgery) used for planning. This process is necessary to calculate the coordinates of each entry point and target in relation to the frame. This CT scan during surgery is not necessary with the use of robotic systems in surgeries called frameless.

The Table 1 presents a comparison between the procedures necessary to perform *frame-based* surgery compared to *frameless* surgeries. The greater number of steps during surgery increases the time needed to perform the surgery and may result in loss of accuracy due to non-deterministic procedures and possible human errors.

Performing a CT scan during surgery is time-consuming. The frame-based process requires a tomography with the stereotactic device immediately after its placement. While having a CT scanner available in the same operating room would streamline logistics, this setup is rarely feasible, as most hospitals do not have a dedicated CT scanner for each operating room. Although some facilities offer operating rooms equipped with CT scanners, their limited availability and competition with other ongoing surgeries complicate scheduling and scalability. As a result, the typical solution is to transport the sedated patient to a separate CT scanner, which increases surgery time and introduces risks of unwanted movement or disturbance to the apparatus during transport, potentially compromising surgical accuracy.

After the tomography with the device, the fusion of intraoperative CT images generated with the device and preoperative MRI images is also a source of errors. In more detail, image fusion consists of aligning two volumes (the set of slices generated in CT and MRI) so that they both represent the same anatomical region. This is necessary because the volume resulting from the CT scanner depends on factors such as the patient's position

Table 1 – Comparison between frame-based and *frameless* procedures for SEEG.

### **Surgery based on stereotactic apparatus**

- 
1. CT, MRI and preliminary surgery exams
  2. Orthogonal trajectory planning based on preliminary evidence before surgery
  3. Start of surgery and fixation of the head in the stereotactic apparatus (Leksell)
  4. Tomography with Leksell and *N-Localizer*
  5. Fusion of CT, MRI and CT images with Leksell to calculate the coordinates of each electrode in relation to the apparatus
  6. Using the stereotactic ruler, drill the skin and skull using a 3 mm drill with an appropriate end point
  7. Fixing the guide screw to the skull
  8. Using the guide screw, insert the temporary stylet into the intracranial space to the target point for electrode guidance
  9. Remove the temporary stylet and, through the guide screw, insert the depth electrode into the intracranial space to the predefined destination
  10. Screw the electrode cover onto the guide screw
  11. Repeat steps 6 to 10 for the remaining electrodes
- 

### **Robot-assisted surgery**

- 
1. CT, MRI and preliminary surgery exams
  2. Planning orthogonal trajectories based on preliminary evidence before surgery using the robot's interface
  3. Facial registration using fiducial points of the face
  4. Positioning the robot and drilling the skin and skull using a 3 mm drill with an appropriate limit stroke
  5. Fixing the guide screw to the skull
  6. Using the guide screw, insert the temporary stylet into the intracranial space to the target point for electrode guidance
  7. Remove the temporary stylet and, through the guide screw, insert the depth electrode into the intracranial space to the predefined destination
  8. Screw the electrode cover onto the guide screw
  9. Repeat steps 4 to 8 for the remaining electrodes
- 

and the coordinate system intrinsic to the CT.

The alignment of the preoperative MRI with the intraoperative CT, in the case of SEEG surgery, allows the planning performed on the MRI to be accurately transferred to the CT acquired with the stereotactic apparatus. In this way, the result of the fusion is the planning of the surgery, containing entry and target points in the same reference as the apparatus images, thus allowing the calculation of the coordinates necessary to align the ruler or stereotactic arc in each trajectory. Even in the most ideal case, this process is not perfect and will contribute to the final error of each trajectory. In summary, the steps of fixing the device, transporting the patient to the CT scanner, and performing image fusion are significant sources of both surgical errors and increased operative time in procedures based on stereotactic devices.



Figure 4 – Robots capable of performing SEEG surgeries: Zimmer Biomet ROSA ONE Brain, Brainlab Cirq and Renishaw Neuromate respectively.

### 3.3.3 Robot-based Surgeries

There are studies in the literature that highlight the development of *frameless* robotic systems for SEEG surgeries, aiming to improve surgical workflow, accuracy, and safety (GONZALEZ-MARTINEZ *et al.*, 2016; CARDINALE FRANCESCO MD *et al.*, 2013). Most of the technical details and innovations in these systems are published as patents rather than in peer-reviewed scientific articles, mainly because of the commercial interests involved.

Renishaw's Neuromate, introduced in 1998, was the first commercially available robot for SEEG neurosurgery (CARDINALE FRANCESCO MD *et al.*, 2013). Fig. 4 shows Neuromate, which features a triangular base and supports for skull fixation using Mayfield or Leksell frames. Subsequently, Medtech (acquired by Zimmer Biomet) developed ROSA ONE Brain, and Brainlab introduced Cirq, both capable of performing SEEG procedures. These systems also support other neurosurgical interventions, including brain biopsies and deep brain stimulation (DBS) for conditions such as Parkinson's disease.

Neuromate was the first commercially available robot for neurosurgery, but its adoption faces significant limitations. A major constraint is the requirement for a dedicated operating room, as the system is not designed for mobility between rooms. This complicates hospital logistics and often prevents acquisition due to infrastructure demands. Additionally, Neuromate features only 5 degrees of freedom (DOF), making it an under-actuated system with reduced mobility and positioning capabilities compared to conventional 6-DOF robotic platforms (KAJITA *et al.*, 2015).

The Cirq robotic system is used with a full neuronavigation system. A device with reflective spheres is fixed to the robot's flange. This device is viewed by an infrared stereo camera and the position of the tool is calculated. Its adjustment is done semi-automatically, where the surgeon approaches the robot to the desired position and the robot adjusts itself with an actuator fixed to its flange. The neuronavigator is used to operate this system, which has: a camera carriage; a screen carriage; and a robotic manipulator fixed to the operating table. Combined with other devices present in the operating room, these three

---

devices bring difficulties in logistics and in organizing the space in the room compared to systems that have only one carriage.

ROSA ONE Brain is not collaborative. In other words, even though it is designed to perform a task together with the surgeon, ROSA does not feature sensors that are present in collaborative systems, such as measuring joint torque, and collision detection with automatic braking. This aspect makes ROSA a conventional robot applied to collaborative tasks, putting doctor and patient higher risk level compared to collaborative systems. Yara, the system proposed in this project, integrates collaborative robots, validated worldwide for tasks that involve joint operations with humans, ensuring the surgeon's and patient's safety.

Typically, non-collaborative industrial robots are required to operate at a safe distance from humans according to workplace safety regulations, but surgical robots are not subject to these industrial standards. Current commercial neurosurgical systems do not incorporate collaborative robotics technology. KUKA pioneered the introduction of collaborative robots for medical applications with the KUKA LBR Med, which is certified according to international medical safety standards. Collaborative systems like these enhance safety during robotic manipulation in surgery, offering advantages over existing non-collaborative platforms.

### 3.4 Introducing Yara

Yara is a collaborative robotic platform designed for frameless intracranial electrode placement procedures, offering increased accuracy, reduced surgical time, and lower risk compared to frame-based methods. The system features a planning software for electrode entry and target points, MRI/CT image fusion, automated patient registration via depth cameras, and collision-free robotic alignment. Additionally, the robot functions as a neuronavigation system, expanding its range of supported neurosurgical procedures such as brain tumor localization and resection.



## 4 DEVELOPMENT

This chapter details the development of the Yara robotic system for SEEG surgery, structured according to the main stages of the surgical workflow. The process begins with the monitoring phase and patient data acquisition (Sec. 4.1), followed by SEEG planning, which encompasses image fusion and electrode placement (Sec. 4.2). Subsequently, the robot-scan registration phase (Sec. 4.3) ensures alignment between the robot and patient anatomy. The SEEG operation phase (Sec. 4.4) describes the integration of robotic assistance for electrode insertion. Finally, the chapter presents the methods and results of system accuracy evaluation and validation (Sec. 5).

### 4.1 Patient Monitoring Phase

Patients exhibiting symptoms suggestive of epileptic seizures, particularly when initial pharmacological treatments are ineffective, undergo comprehensive monitoring using continuous video-EEG and MRI. Video-EEG (see Sec. 3.2.1) enables the recording of electrical brain activity synchronized with video, facilitating the identification of abnormal patterns and correlation with clinical events. MRI provides high-resolution anatomical images, aiding in the localization of potential epileptogenic zones. Together, these diagnostic tools are essential for gathering evidence, accurately classifying the type of epilepsy, and informing subsequent treatment strategies.

During the monitoring phase, patients may remain hospitalized for several days to allow comprehensive diagnostic evaluation and formulation of a treatment plan. A key objective is to determine whether the epilepsy is focal and to localize the epileptogenic focus. MRI and EEG data are analyzed to identify the precise region responsible for seizure onset. If the epilepsy is determined to be focal, surgical treatment may be considered depending on the location of the focus—specifically, whether it is situated within brain regions considered safe for surgical intervention and not in eloquent zones responsible for critical functions such as language, motor, or sensory processing. If surgery is deemed viable, invasive techniques like SEEG or ECoG are considered, with SEEG offering distinct advantages as discussed in Sec. 3.3. Once SEEG is selected as the preferred approach, the Yara robotic system supports the surgical workflow, beginning with precise planning of electrode trajectories.

### 4.2 SEEG Planning Phase

The user interface is prepared for SEEG planning, developed to address neurosurgeons' and neurologists' needs during planning. The goal of planning is to select target

points so that the electrodes cross the most probable epileptogenic zone. Entry points need to be selected so that the electrode trajectory is safe and follows a path without collision with critical structures such as arteries or eloquent regions of the brain. Typically, electrodes have between 5 and 15 contacts along their length, spaced by a couple of millimeters. Between 5 and 10 electrodes are placed in the SEEG procedure.

For SEEG planning, the surgeon requires high-resolution MRI images to visualize soft tissues, brain structures, and vascularization, as well as CT images that provide precise information about the skull. Combining these modalities through image fusion enables the simultaneous assessment of critical anatomical features—such as blood vessels, gray and white matter, and bone structures—in a unified reference frame. This alignment is essential for safe and effective electrode placement, as it allows the surgeon to avoid critical regions and optimize the trajectory of each electrode.

#### 4.2.1 Image Fusion

For image fusion, we adopted the method described in (KLEIN *et al.*, 2009), which enables the alignment of CT-CT, MRI-MRI, or CT-MRI images. The fusion process aims to optimize the mutual information metric, identifying the transformation that best aligns a source image with a target image. In multimodal fusion scenarios such as CT-MRI, the images differ in tissue representation and contrast — bone appears bright in CT but is nearly invisible in MRI. Mutual information serves as a statistical measure of the shared information between two random variables. In image registration, it quantifies how well one image explains the other, independent of intensity values, making it effective for multimodal image alignment.

#### 4.2.2 Electrode Placement

After analyzing the images, electrodes can be planned by determining the entry and target points, the type of electrode containing basic information such as spacing, coordinates, number of contacts, and the dimensions of each electrode. This step is performed a couple of days before the surgery; the planned electrode is saved and loaded on the day of the surgery into the interface. Small adjustments can be made during the surgery if needed.

### 4.3 Robot-Scan Registration Phase

Before starting the operation, it is essential to perform a registration procedure to align the coordinate systems of the preoperative scans and the robot. This step ensures that the positions of the planned electrode trajectories correspond accurately to the physical space in which the robot operates. The registration method adopted in this work is known as *fiducial registration*, which involves identifying and matching a set of

anatomical or artificial landmarks (fiducials) in both the image space and the physical space. By determining the transformation that best aligns these corresponding fiducial points, the system can accurately map planned positions from the imaging data to the robot's coordinate system (ZENG *et al.*, 2017). This alignment is fundamental for transferring surgical plans to the robotic system and ensuring precise execution during the procedure.

The procedure begins by identifying several fixed anatomical or artificial landmarks, known as fiducial points, within the preoperative images. These same points are then physically located on the patient using the robotic arm. To record each corresponding point, the operator positions the robot's tool at the desired location and confirms the selection using the flange button on the robot's end effector. The collected coordinates are transmitted to the robot's control module, which computes the optimal rigid transformation using the ICP method. Communication between the Yara system and the robot controller occurs over a TCP/IP network, with structured message categories and commands to ensure reliable data exchange throughout the registration process.

Expanding on the ICP method by (GAO *et al.*, 2017), the goal is to find the matrix  $\mathbf{R}$  and vector  $\mathbf{t}$  that best solve the Euclidean transformation 4.1 given a matched set of 3D points like  $\mathbf{P} = \{\mathbf{p}_1, \dots, \mathbf{p}_n\}$  and  $\mathbf{P}' = \{\mathbf{p}'_1, \dots, \mathbf{p}'_n\}$ .

$$\forall i, \mathbf{p}_i = \mathbf{R}\mathbf{p}'_i + \mathbf{t} \quad (4.1)$$

In this procedure, fiducial landmarks are selected—these are anatomically distinct and reproducible points on the patient's head that can be reliably identified both in the CT/MR images and in the physical space. Commonly used fiducials include the nasion (the indentation between the forehead and the nose), the left and right preauricular points (just in front of each ear), and sometimes additional points such as the tip of the nose or the outer canthi of the eyes. These landmarks are chosen for their ease of identification and minimal movement relative to the skull avoiding soft tissue deformation.

The system computes the transformation  ${}^{robot}T_{scan}$  that best aligns the two sets of points, minimizing the reprojection error and ensuring that the planned trajectories in the image space correspond precisely to the patient's anatomy in the real world. The reprojection error is computed by transforming the fiducial points in the source space to the target space (robot space) and comparing with the collected fiducials in the target space (Equation 4.2).

$${}^{robot}P_{c proj} = {}^{robot}T_{scan} {}^{robot}P_{c scan} \quad (4.2)$$

$$Reproj = ||{}^{robot}P_{c robot} - {}^{robot}P_{c proj}|| \quad (4.3)$$

#### 4.4 Intra-Operation Phase

The next step is the surgery for the precise placement of electrodes in the patient. In the operating room, strict safety protocols are essential, as any unintended movement or error can pose risks to the patient, staff, or equipment. To address this, the Yara system incorporates a digital twin of the robot within its interface, providing real-time visualization of the robot's position and movements. Before executing any planned motion, the system displays the intended trajectory and requires explicit confirmation from the operator. This workflow ensures that each step of the surgical process is performed with maximum safety and situational awareness.

During the drilling process, the Yara system assists the surgeon by displaying the precise drilling depth required to safely penetrate the skull without breaching the *dura-mater*. Once the bone has been traversed, a drill guide is positioned to maintain the correct trajectory and stabilize the electrode. The interface then provides the exact insertion depth needed for the electrode to reach the planned intracerebral target, ensuring accurate and safe placement.

## 5 METHOD AND RESULTS

As discussed in Sec. 3.3, an SEEG method must be sufficiently accurate to place each electrode at the planned position and orientation. The accuracy can be measured by the Euclidean distance between the planned entry point and the entry point achieved after the surgery. The same method applies to the target point. The angle between the entry-to-target vector  $\vec{P_{target}} - \vec{P_{entry}}$  for the planned electrodes and the post-surgery electrodes reflects the orientation error.

To comprehensively assess the accuracy of Yara system for SEEG surgeries, we developed and tested three distinct phantom models, each with a dedicated evaluation setup: (1) a conical target phantom in a simulated environment, (2) a synthetic brain phantom in a simulated environment, and (3) a synthetic brain model assessed under actual surgical room conditions.

The experiments were conducted in a controlled laboratory environment designed to closely mimic the conditions of an actual operating room. This setup included a surgical table, a head clamp for securing the phantom or synthetic head, and the complete robotic system mounted on its dedicated cart. The laboratory environment allowed for iterative testing and refinement of the workflow, ensuring that all components of the system functioned as intended before transitioning to a clinical setting.

Following laboratory assessments, the system was evaluated in a real surgical room at the Hospital das Clínicas da Faculdade de Medicina de Ribeirão Preto (HC-FMRP-USP). In this environment, the robot and its cart were transported and installed according to standard operating room protocols. The tests in the surgical room aimed to assess the system’s performance under actual clinical conditions, including the presence of medical staff, and integration with existing surgical infrastructure.

### 5.1 Conical Target Phantom in Simulated Environment

To validate the system’s accuracy using a *phantom*, we employed a 3D-printed phantom of a child’s head along with a base containing cylinders topped with cones (the patient data used for the phantom model was approved for research use, and no personal or identifiable information is available). The apex of each cone served as a target point, requiring the system to position a thin metal rod — simulating an electrode — precisely at these locations. During the planning phase, entry points were arbitrarily distributed across the skull surface to maximize variability, while target points corresponded to the cone peaks. Registration was performed using fiducial markers placed on the head surface, following the same protocol as the synthetic brain validation.

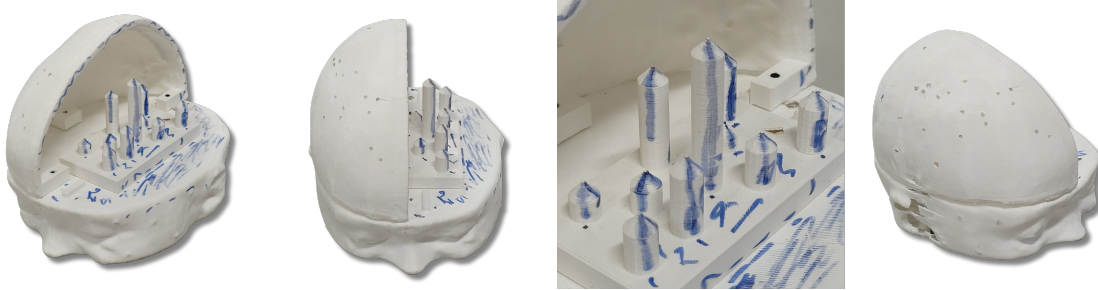


Figure 5 – Conical targets phantom used for quantitative accuracy assessment via stereoscopic imaging.

During the operation phase, the robot sequentially positioned itself at each planned electrode site. The interface provided the required drilling depth, guiding the placement of the drill stop, and calculated the insertion length needed for the rod to reach the target point.

To measure the accuracy of the system, we utilized a stereo camera setup to capture images of the phantom after rod insertion. The stereo camera allowed for precise measurement of the distance between the tip of the inserted rod and the apex of each cone, representing the planned target point.



Figure 6 – Conical targets phantom in simulated environment for metal rods positioning using the robotic system.

The stereo image pair was acquired using a rectified stereo camera with a 4 cm baseline and a resolution of  $1920 \times 1080$  pixels, with known intrinsic parameters. The tip of the rod and the cone apex were manually marked in both images, with an average marking error of proportional to the depth. We assumed a linear disparity pixel error (the error of a point in the left image and its corresponding point in the right image) of 0 to 5 pixels from 0 to 2.5 meters. The depth error was calculated using the Formula 5.1, where  $z$  is the depth,  $e_{\text{disp}}$  is the disparity error in pixels,  $b$  is the distance between the cameras in meters, and  $f_x$  is the focal length in pixels.

$$\Delta Z = \frac{z^2 \cdot e_{\text{disp}}}{b \cdot f_x} \quad (5.1)$$

Using the Eq. 5.1, it was possible to estimate a maximum measurement error of

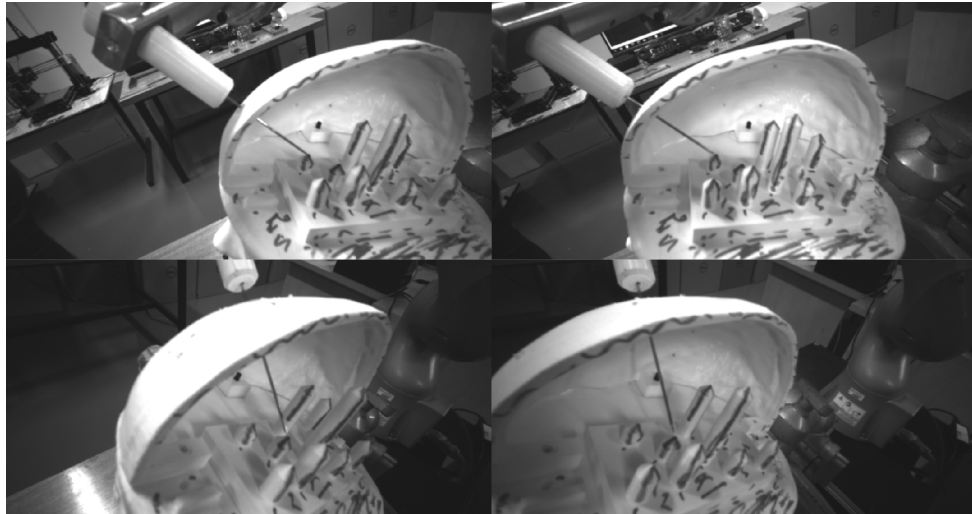


Figure 7 – Examples of stereo camera images used to measure the distance between the metal rod tip and the planned target point. The top and bottom rows show the left and right images of a stereo pair for the same moment in time.

Electrode	1	2	3	4	5	6	7	8	9	Mean
$\Delta$ Target (mm)	1.5	1.3	2.7	1.6	2.5	2.3	1.1	1.9	1.4	$1.8 \pm 0.3$

Table 2 – Error in the positioning of target points planned and reached after surgery using a model with phantom and stereo camera to measure distances.

0.3 mm, which corresponds to the largest expected uncertainty in the distance calculation due to stereo camera disparity error. Nine electrodes were inserted, followed by the target error estimation process. Fig. 6 presents the model with the phantom and Fig. 7 presents images from the stereo camera used to calculate the error. Table 2 presents the target error for each electrode, resulting in an average error of  $1.8 \pm 0.3$  mm.

## 5.2 Synthetic Brain Phantom in Simulated Environment



Figure 8 – Phantom model with synthetic brain produced using silicone rubber and 3D printed plastic surface skin after electrode placement.

To further evaluate the system, tests were conducted using a synthetic brain phantom. The model was created by 3D printing the surface of a patient's head and molding the right hemisphere of the brain from silicone to closely mimic the anatomical structure and consistency of real brain tissue.



Figure 9 – Synthetic brain phantom in the simulated environment during electrode placement with the robotic system. The rightmost image displays the postoperative CT scan of inserted electrodes.

A 3D-printed positive model of the brain was produced from patient imaging data. This positive was used to create a negative mold using silicone rubber. Once cured, the negative mold was filled with silicone rubber of Shore A 5 hardness, chosen to approximate the mechanical properties of brain tissue. To facilitate demolding, a release agent was applied to the mold surface. The resulting synthetic brain was then positioned inside the 3D-printed head model, which incorporated a section of the skull to closely replicate the patient anatomy (Figure 8).

Preoperative CT scan and a surgical plan were used to replicate the clinical scenario in a controlled laboratory environment. The robotic system was then employed to insert nine electrodes according to the planned trajectories. The procedure was completed successfully, demonstrating the system’s ability to perform electrode placement in a surgical simulation.

After the operation, the phantom with the electrodes placed invasively was taken for tomography to acquire images that show the internal positioning of the electrodes. Through this, it was possible to compare the positioning of the inserted electrodes with the surgical planning and the desired trajectories for each electrode, seeking to calculate the system error. As presented in Section 3.2, the error between the planned entry and target points and those achieved postoperatively are evaluation metrics for SEEG surgery and were calculated in this process.

Figure 8 shows the synthetic model developed. The comparison between the planned and achieved electrodes with the fusion of the postoperative CT with the preoperative images (Figure 10) allows the calculation of Euclidean distances between the planned and achieved trajectories and, therefore, allows the evaluation of the system’s accuracy (Table 3). The CT volume has a slice spacing of 0.25 mm on the three dimensions between slices, used as the measurement error.

Some limitations were observed during the tests, particularly regarding the adhesion between the electrodes and the silicone rubber material. This adhesion increased friction and made electrode insertion more difficult compared to real brain tissue, where such resistance is not typically encountered. As a result, the insertion process in the phantom did

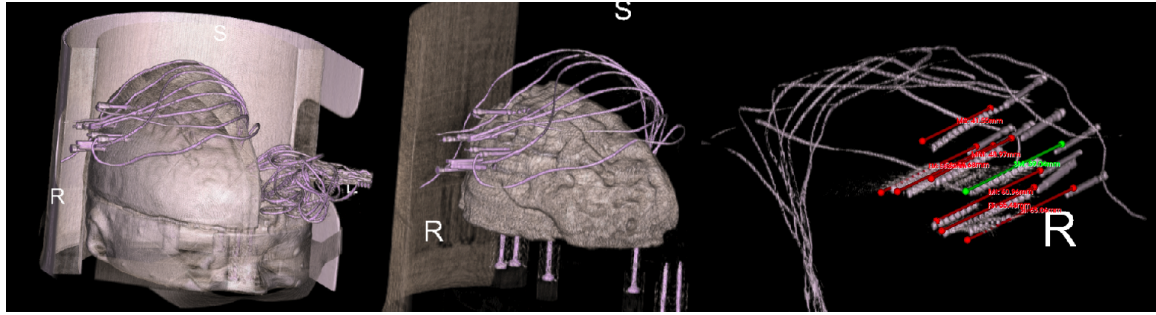


Figure 10 – Comparison between preoperative (red and green lines) and postoperative (gray contacts) electrode trajectories using CT scan of the synthetic brain model in the simulated environment.

Electrode	1	2	3	4	5	6	7	Mean
$\Delta\text{Entry}$ (mm)	1.47	1.81	1.58	1.71	0.56	0.95	1.04	$1.30 \pm 0.25$
$\Delta\text{Target}$ (mm)	2.57	2.62	3.72	2.26	4.88	3.48	1.97	$3.07 \pm 0.25$

Table 3 – Error in positioning the entry and target points planned and reached after surgery using a synthetic brain model.

not fully replicate the ease of electrode placement observed in clinical practice. Nevertheless, the synthetic brain phantom provided a reliable platform for simulating electrode placement and quantitatively assessing system accuracy under controlled conditions.

### 5.3 Synthetic Brain Phantom in Surgical Room

In order to evaluate the system in a real surgical environment, a second synthetic brain model was created. For this phantom, we produced a brain of alginate to better simulate the consistency of real brain tissue. The surface of the head was again 3D printed to replicate the anatomical structure. The phantom was taken to the operating room, where the robotic system was used to perform electrode placement under actual surgical conditions, including the presence of medical staff and adherence to operating room protocols.

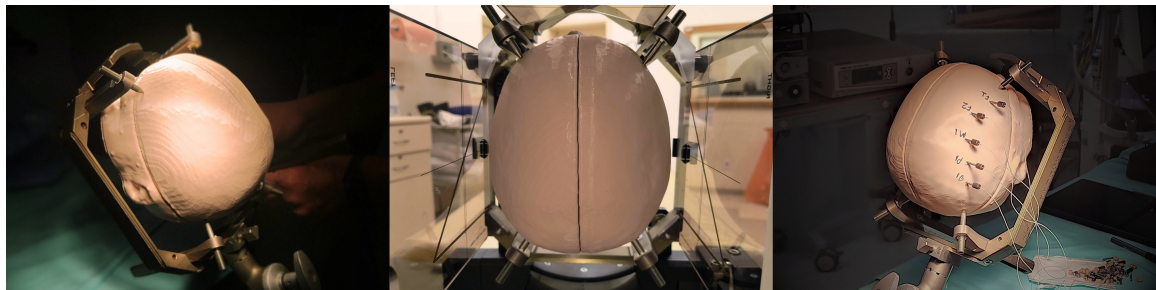


Figure 11 – Phantom model with synthetic brain placed in the surgical room using stereotactic frame for electrode placement.

In the right brain hemisphere, we introduced the electrodes using stereotactic frame guidance, while in the left hemisphere, the procedure was performed using the robotic

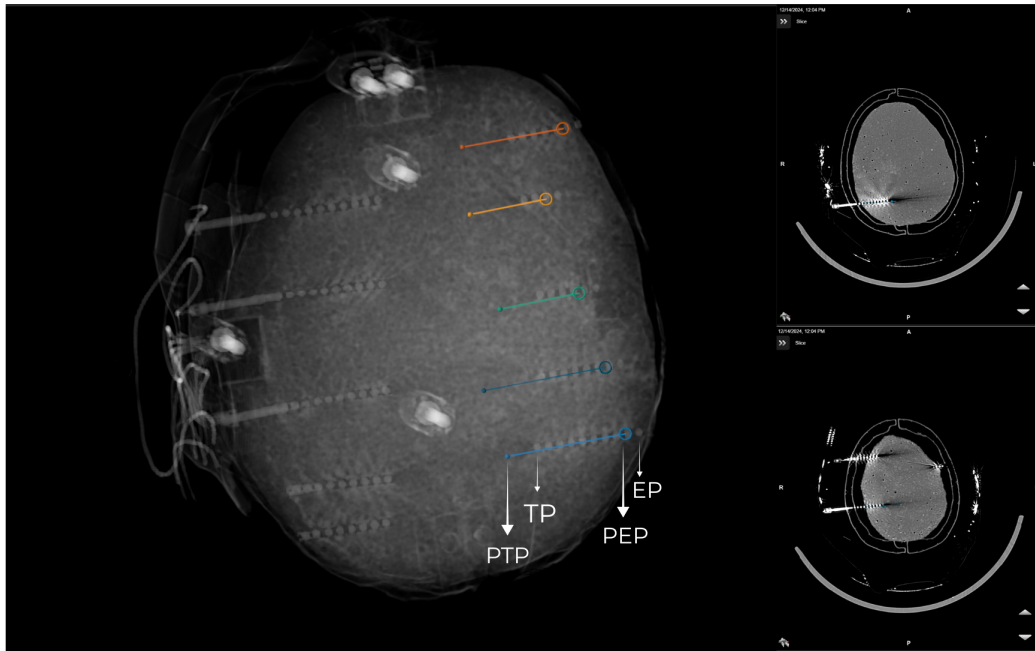


Figure 12 – Comparison between frame-based planned electrode trajectories (color lines) and those achieved after surgery (showed by the sliced view of the contacts in bright gray) using CT scan of a synthetic brain model in OR with stereotactic frame.

system. This approach allowed for a direct comparison between the traditional frame-based method and the robotic-assisted technique within the same surgical setting. After the procedure, a CT scan was performed to visualize the internal positioning of the electrodes. The postoperative CT images were then fused with the preoperative planning images to assess the accuracy of electrode placement.

For the stereotactic frame procedure, electrode trajectories were planned using preoperative MRI images. In the operating room, the stereotactic frame was securely attached to the phantom's head with the N-Localizer (see Sec. 3.3.2) and the assembly was transported to the CT scanner for image acquisition. The acquired CT images were fused with the preoperative MRI, enabling precise calculation of electrode coordinates within the frame's coordinate system. Electrode insertion was then performed sequentially, guided by the stereotactic apparatus (Fig. 11). Finally, a postoperative CT scan was conducted to verify the actual positions of the electrodes (Fig. 12), fused with the preoperative images, and entry and target errors were calculated (Tab. 4).

Electrode	1	2	3	4	5	Mean
$\Delta$ Entry (mm)	1.6	2.1	1.8	3.6	5.0	$2.8 \pm 0.25$
$\Delta$ Target (mm)	8.1	16.2	11.1	15.3	13.9	$12.9 \pm 0.25$

Table 4 – Error in positioning the entry and target points planned and reached after surgery using a synthetic brain model in the surgical room with stereotactic frame.

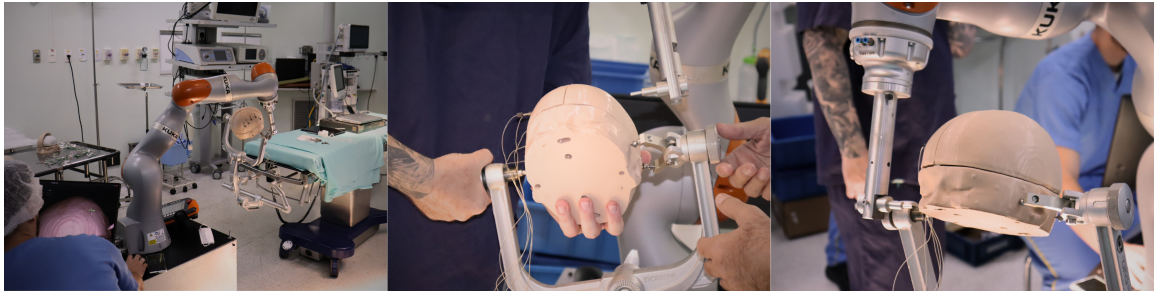


Figure 13 – Operating room (OR) with synthetic brain phantom ready for electrode placement using the robotic system.



Figure 14 – Electrodes fixed to the synthetic brain phantom in OR with robotic system.

For the robotic procedure, the same preoperative MRI images served as the basis for planning. The phantom was stabilized in the Mayfield head clamp, and fiducial markers were affixed to the surface for registration (Fig. 13). The robot autonomously positioned itself at each planned electrode site, and electrodes were inserted along the preplanned trajectories (Fig. 14). Unlike the frame-based approach, no intraoperative CT scan was required, as registration was accomplished directly using the anatomical fiducial markers.

Electrode	1	2	3	4	5	Mean
ΔEntry (mm)	3.1	3.7	2.9	3.2	2.6	$3.1 \pm 0.25$
ΔTarget (mm)	5.8	5.9	5.8	5.9	5.5	$5.8 \pm 0.25$

Table 5 – Error in positioning the entry and target points planned and reached after surgery using a synthetic brain model in the OR with robotic system.

As in the frame-based procedure, postoperative CT images were fused with pre-operative MRI to evaluate electrode placement accuracy. Entry and target errors were calculated by comparing planned and actual electrode positions (Fig. 15, Tab. 5).

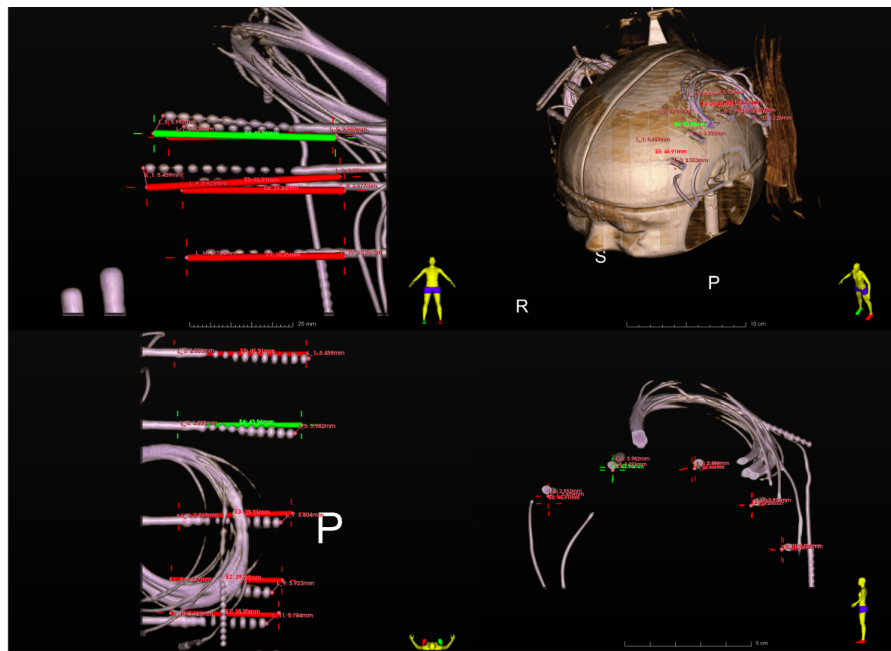


Figure 15 – Comparison between planned electrode trajectories (red and green lines) and those achieved after surgery (3D contacts in gray) using CT scan of a synthetic brain model in OR with robotic system.

## 6 DISCUSSION AND CONCLUSION

The literature indicates that frame-based SEEG procedures can achieve a maximum entry point error (EPE) of 7.1 mm and target point error (TPE) of 8.5 mm, as documented in (GIRGIS *et al.*, 2020). Some studies have observed lower average errors, with EPE values of 1.51 mm and TPE values of 1.59 mm, which may be related to variations in surgical technique, image fusion accuracy, or other procedural factors. Robotic-assisted SEEG procedures have demonstrated comparable accuracy, with reported EPE and TPE values of 1.38 mm and 1.54 mm, respectively. In terms of operative duration, robotic-assisted surgeries have been shown to be more efficient, with an average time of 127 minutes compared to 152 minutes for frame-based methods (ZHENG *et al.*, 2021).

The conical targets phantom focused on evaluating the target error caused by intrinsic sources. These sources are defined as the internal aspects of the systems that can generate inaccuracies, such as the robot's kinematics, the end effector tool tolerances, robot cart movements and vibrations, and the registration method. Since no electrode insertion was performed, errors related to the surgical procedure, such as brain shift and electrode bending, were not present in the results. The phantom tests resulted in an average TPE of 1.8 mm, which are comparable to the values reported in the literature for robotic-assisted SEEG procedures.

The synthetic brain phantom test was designed to assess the overall system accuracy by incorporating both intrinsic and extrinsic sources of error. Extrinsic factors include procedural elements such as electrode bending, manual depth measurement inaccuracies, and interactions between the electrode and the synthetic brain material. The results indicated an average EPE of 1.3 mm and TPE of 3.1 mm. While the EPE is consistent with values reported for robotic-assisted SEEG procedures in the literature, the slightly elevated TPE may be attributed to these additional extrinsic factors, particularly the friction and adherence between the electrode and the synthetic brain, which could have contributed to deviations during insertion.

The frame-based errors observed in this study (Sec. 5.3) were higher than other studies (ZHENG *et al.*, 2021), primarily attributed to inaccuracies in the depth dimension. These discrepancies may be related to the properties of the synthetic brain model made of alginate, which may not perfectly replicate the mechanical resistance and consistency of real brain tissue. Additionally, a systematic error may have been introduced during the manual calculation of the insertion depth, further contributing to the deviation between planned and achieved electrode positions. Since the focus of this work was not on the frame-based method, a detailed analysis of these deviations was not conducted.

The robotic-assisted method simulation with the synthetic brain in OR (Sec. 5.3) demonstrated an average EPE of 3.1 mm and TPE of 5.8 mm, which are higher than the earlier phantom tests. This increase in error can be attributed to the additional extrinsic factors present in the OR environment. The mayfield head clamp used to fix the phantom has a larger length compared to the one used in the previous tests. With a longer clamp, the phantom bended more easily during the drilling of the skull, increasing the EPE, modifying the entry angle and, therefore, contributing to the TPE. To further avoid this source of error, a rigid and stable attachment between the robot based and the patient head could be designed.

The Yara system represents a significant advancement in robotic assistance for neurosurgery. This work demonstrates Yara's robust performance and reliability, paving the way for its future application in brain biopsy and DBS surgeries. The main contributions include the development of a versatile, cost-effective robotic platform, comprehensive validation using both phantom and synthetic brain models, and the integration of planning and registration methods. With continued validation and clinical trials, Yara has the potential to become widely available in hospitals, offering a safe, precise, and accessible solution for a range of neurosurgical interventions.

## REFERENCES

- BEGHI, E. The epidemiology of epilepsy. **Neuroepidemiology**, S. Karger AG Basel, Switzerland, v. 54, n. 2, p. 185–191, 2020.
- BEGHI, E. *et al.* Recommendation for a definition of acute symptomatic seizure. **Epilepsia**, Wiley Online Library, v. 51, n. 4, p. 671–675, Apr 2010.
- Blausen.com staff. Medical gallery of blausen medical 2014. **WikiJournal of Medicine**, v. 1, n. 2, 2014. ISSN 2002-4436.
- CARDINALE FRANCESCO MD, P. *et al.* Stereoelectroencephalography: Surgical methodology, safety, and stereotactic application accuracy in 500 procedures. **Neurosurgery**, v. 72, n. 3, p. 353–366, March 2013.
- DASGUPTA, D. *et al.* Previous, current, and future stereotactic eeg techniques for localising epileptic foci. **Expert Review of Medical Devices**, Taylor & Francis, v. 19, n. 7, p. 571–580, Jul 2022.
- FIANI, B. *et al.* Stereoelectroencephalography versus subdural electrode implantation to determine whether patients with drug-resistant epilepsy are candidates for epilepsy surgery. **Neurol Med Chir (Tokyo)**, Neurol Med Chir, v. 61, n. 6, p. 347–355, 2021.
- FISHER, R. S. *et al.* Epileptic seizures and epilepsy: definitions proposed by the international league against epilepsy (ilae) and the international bureau for epilepsy (ibe). **Epilepsia**, Wiley Online Library, v. 46, n. 4, p. 470–472, Apr 2005.
- GAO, X. *et al.* 14 lectures on visual slam: From theory to practice. Publishing House of Electronics Industry, 2017.
- GIRGIS, F. *et al.* Superior accuracy and precision of seeg electrode insertion with frame-based vs. frameless stereotaxy methods. **Acta Neurochirurgica**, Springer, v. 162, n. 10, p. 2527–2532, 2020.
- GONZALEZ-MARTINEZ, J. *et al.* Technique, results, and complications related to robot-assisted stereoelectroencephalography. **Neurosurgery**, v. 78, p. 169–180, 2016.
- IORDANOU, J. C. *et al.* Approach angle affects accuracy in robotic stereoelectroencephalography lead placement. **World Neurosurgery**, Elsevier Inc, v. 128, p. e322–e328, 2019. ISSN 18788769. Available at: <https://doi.org/10.1016/j.wneu.2019.04.143>.
- JEHI, L. *et al.* Comparative effectiveness of stereotactic electroencephalography versus subdural grids in epilepsy surgery. **Annals of neurology**, Wiley, v. 90, n. 6, p. 927–939, 2021.
- JONES, J. C. *et al.* Techniques for placement of stereotactic electroencephalographic depth electrodes: Comparison of implantation and tracking accuracies in a cadaveric human study. **Epilepsia**, v. 59, p. 1667–1675, 2018. ISSN 15281167.

KAEWBORISUTSAKUL, A. *et al.* Usefulness of robotic stereotactic assistance (rosa®) device for stereoelectroencephalography electrode implantation: A systematic review and meta-analysis. **Neurologia medico-chirurgica**, The Japan Neurosurgical Society, v. 64, n. 2, p. 71–86, 2024.

KAJITA, Y. *et al.* Installation of a neuromate robot for stereotactic surgery: Efforts to conform to Japanese specifications and an approach for clinical use-technical notes. **Neurologia medico-chirurgica**, Japan Neurosurgical Society, v. 55, n. 12, p. 907–914, 2015. Available at: <https://doi.org/10.2176/nmc.tn.2015-0043>.

KLEIN, A. *et al.* Evaluation of 14 nonlinear deformation algorithms applied to human brain MRI registration. **NeuroImage**, Elsevier, v. 46, n. 3, p. 786–802, 2009.

LESSER, R.; CRONE, N.; WEBBER, W. Subdural electrodes. **Clin Neurophysiol**, Elsevier, v. 121, n. 9, p. 1376–1392, 2010.

LOZANO, A. *et al.* **Textbook of Stereotactic and Functional Neurosurgery**. Springer, 2009. (Textbook of Stereotactic and Functional Neurosurgery, v. 1). ISBN 9783540699590. Available at: <https://books.google.com.br/books?id=cnF-2KCeR1sC>.

MAZOYER, B. In memoriam: Jean Talairach (1911–2007): a life in stereotaxy. **Human brain mapping**, v. 29, n. 2, p. 250–252, Feb 2008.

MILLER, J. W.; HAKIMIAN, S. Surgical treatment of epilepsy. **Continuum (Minneapolis Minn)**, v. 19, n. 3 Epilepsy, p. 730–742, Jun 2013.

NGUGI, A. *et al.* Estimation of the burden of active and life-time epilepsy: a meta-analytic approach. **Epilepsia**, Wiley, v. 51, n. 5, p. 883–890, 2010.

ROJAS-VILLABONA, A. *et al.* Evaluation of the stability of the stereotactic Leksell frame g in gamma knife radiosurgery. **Journal of applied clinical medical physics / American College of Medical Physics**, v. 17, p. 5944, 05 2016.

SARMAST, S. T.; ABDULLAHI, A. M.; JAHAN, N. Current classification of seizures and epilepsies: Scope, limitations and recommendations for future action. **Cureus**, Cureus Inc., v. 12, n. 9, p. e10549, 2020.

SHEN, Y. Machine learning based epileptic seizure detection for responsive neurostimulator system optimization. **Journal of Physics: Conference Series**, v. 1453, p. 012089, 01 2020.

SUN, C.; MOU, C. Survey on the research direction of EEG-based signal processing. **Frontiers in Neuroscience**, v. 17, 2023. ISSN 1662-453X. Available at: <https://www.frontiersin.org/journals/neuroscience/articles/10.3389/fnins.2023.1203059>.

ZENG, B. *et al.* A surgical robot with augmented reality visualization for stereoelectroencephalography electrode implantation. **International journal of computer assisted radiology and surgery**, Springer, v. 12, n. 8, p. 1355–1368, 2017.

ZHENG, J. *et al.* Robot-assisted versus stereotactic frame-based stereoelectroencephalography in medically refractory epilepsy. **Neurophysiologie Clinique**, Elsevier, v. 51, n. 2, p. 111–119, 2021.